Rare Met. (2023) 42(6):2000–2006
https://doi.org/10.1007/s12598-018-1069-z

RARE METALS
www.editorialmanager.com/rmet

Magnetic field annealing of FeCo-based amorphous alloys to enhance thermal stability and Curie temperature

Zai-Dao Li, Wei-Wei Zhang, Ge-Tian Li, Song-Song Li, Hong-Sheng Ding, Tao Zhang, Yu-Jun Song*

Received: 13 February 2017 / Revised: 30 April 2017 / Accepted: 14 May 2018 / Published online: 23 June 2018

Abstract Annealing temperatures and applied magnetic fields are two important parameters for the performance modification of magnetic alloys. This article investigated the effect of different annealing temperatures on crystallization condition, magnetic properties and thermal stability of the amorphous magnetic alloy $Co_{36}Fe_{36}Si_{4.8}B1_{9.2}Nb_4$ (at%). Results indicate that the annealing temperature can significantly affect the size and content of precipitated nanocrystals in the amorphous alloy, and the precipitation of nanocrystalline phases can result in the distinct change of magnetic properties and Curie temperature. When the annealing was performed at 595 °C for 30 min under an applied transverse external magnetic field of 9550.0 $A{\cdot}m^{-1}$, the amorphous alloy shows excellent soft magnetic properties with the saturation magnetization of alloy reaching 110.00 $mA{\cdot}m^2{\cdot}g^{-1}$, the residual magnetic induction intensity of 4×10^{-6} T and the coercivity as low as 57.3 $A{\cdot}m^{-1}$. Furthermore, the Curie temperature of the field-annealed samples can reach up to 440 °C, approximately 58 °C higher than that of the as-quenched species.

Keywords Soft magnetic alloys; Amorphous alloy; Field annealing

1 Introduction

Nanocrystalline soft magnetic alloy usually refers to single-phase or multi-phase polycrystalline alloys with a grain size of 1–100 nm [1–4] and is characterized by high magnetic induction, high permeability, low core loss and low-cost production [5–7]. The extensive production of nanocrystalline soft magnetic materials marked the development of magnetic materials [8]. However, studies show that the Curie temperature (T_C) of nanocrystalline alloys is relatively low, which limits their application [9–12]. Improving T_C of such alloys is critical by considering the rapid growth of the electronic industry, which requires soft magnetic materials to work reliably at high temperature and frequency. Magnetic field heat treatment has been reported as an effective tool for modifying the microstructure of amorphous alloys [13–16], and changes in microstructures can affect the magnetic properties and thermal stability of the alloys dramatically [17]. The present study mainly investigates the effect of annealing temperature in magnetic field heat treatment on T_C and magnetic properties of amorphous alloys using CoFe amorphous alloys as a model alloy.

In this work, $Co_{36}Fe_{36}Si_{4.8}B1_{9.2}Nb_4$ (at%) amorphous alloys were prepared by planar flow casting. The crystallization behavior, magnetic properties, thermal properties and T_C of the amorphous alloys before and after annealing were characterized. The samples were annealed under a transverse magnetic field of about 9550.0 $A{\cdot}m^{-1}$. Effects of annealing temperatures on crystallization behavior of the alloys, their magnetic properties and T_C were investigated.

Zai-Dao Li and Wei-Wei Zhang have contributed to this article equally.

Z.-D. Li, W.-W. Zhang, G.-T. Li, S.-S. Li, H.-S. Ding, Y.-J. Song*
Center for Modern Physics Technology, Department of Applied Physics, Beijing Key Laboratory for Magneto-Photoelectrical Composite and Interface Science, University of Science and Technology Beijing, Beijing 100083, China
e-mail: songyj@ustb.edu.cn

Z.-D. Li, T. Zhang
School of Materials Science and Engineering, Beihang University, Beijing 100191, China

2 Experimental

2.1 Fabrication of CoFe-based amorphous alloy

The Co-rich amorphous alloys were prepared by rapid solidification of liquid metal. An alloy ingot with a composition of $Co_{36}Fe_{36}Si_{4.8}B1_{9.2}Nb_4$ was first prepared using a high-frequency induction melting process (NEW-ADR-05), where bulk cobalt (99.98%), iron (99.8%), silicon (99%), boron (99.999%) and niobium (99.999%) were melted to produce an alloy. To ensure that the sample melted evenly, the ingot was re-melted three to five times under an Ar atmosphere. The ingot was re-melted again and sprayed directly to the copper wheel surface at a rotation speed of 3000 r·min^{-1} [18], forming amorphous ribbons with the width of ~ 3 mm and the thickness of ~ 30 μm.

2.2 Field annealing of Co-based amorphous alloy

Homemade heat treatment apparatus was utilized for the field annealing of the Co-based amorphous alloy in the experiment. The equipment is composed of a heating quartz tube, temperature controller, thermocouple, controlled gas supply flow meter and Helmholtz coil system, which can provide a controllable magnetic field. The sample was placed in the middle of one quartz tube. The temperature of the quartz tube was controlled with a set temperature profile under a transverse magnetic field of about 9550.0 A·m^{-1}. The samples were annealed at a desired annealing temperature for 30 min; the temperature of the samples was detected by the thermocouple, and then they were allowed to cool down to room temperature. During annealing, the inert Ar gas was supplied at a certain flow rate to prevent oxidation of the samples.

2.3 Structure and thermal characterization of prepared CoFe-based alloys

In this study, the structure of quenched and annealed samples was determined with X-ray diffractometer (XRD, Bruker AXS D8) using Cu Kα radiation (λ = 0.15418 nm). Differential scanning calorimetry (DSC; NETZSCH, Selb, Germany) was used to carry out thermal analysis and test of quenched and annealed samples at a scanning rate of 20 K·min^{-1}, and the crystallization ratio of the amorphous alloy can also be estimated.

2.4 Characterization of magnetic properties of alloys

The hysteresis loops of the prepared ribbon-shaped samples were measured by a vibration sample magnetometer (VSM, LakeShore 7404), and the average value of coercivity (H_c) and saturation magnetization (M_s) was accurately determined by an accuracy of ± 159.1 A·m^{-1} and ± 3 mA·m^2·g^{-1} after measuring three times. The Curie temperatures of the prepared CoFe-based alloys were characterized by a self-assembled magnetic force-coupled thermal gravimetric analyzer (MF-TGA), which can provide an applied magnetic field during the heating process. Because the samples are ferromagnetic materials, the external magnetic field has an attractive force to them. When the temperature rises above the Curie temperature, the attractive force has a change led by the magnetic transition of the sample.

3 Results and discussion

Thermal properties of the as-spun samples were first characterized by DSC and TGA to determine the suitable annealing temperatures. As shown in Fig. 1, the glass transition temperature (T_g) is 517 °C and the onset temperatures of the first and second crystallization events are 595 °C (T_{x1}) and 755 °C (T_{x2}), respectively. Consequently, 520, 550, 595 and 675 °C were selected to study the effects of annealing temperature on the crystallization and thermal stability of the alloys. The room temperature hysteresis loop of the as-spun alloy is shown in Fig. 2, giving coercivity (H_c) of 78.0 A·m^{-1} and saturation magnetism (M_s) of 102.9 mA·m^2·g^{-1}. Therefore, the annealing field was selected as 9550.0 A·m^{-1} (above its M_s) in order to obtain an efficient field annealing effect. The suitable forces for the measurement of the Curie temperature were also determined by the hysteresis loop.

XRD was utilized to analyze the crystallization of the samples annealed at different temperatures under a transverse magnetic field. Figure 3 shows that the as-quenched sample exhibits only one broad peak at approximately 45°,

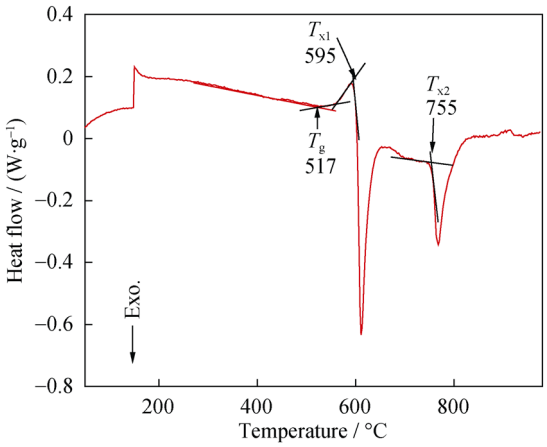

Fig. 1 DSC curve of quenched $Co_{36}Fe_{36}Si_{4.8}B1_{9.2}Nb_4$ amorphous alloy

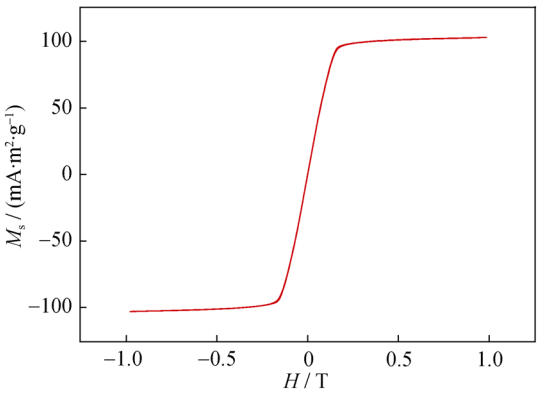

Fig. 2 Hysteresis loop of as-spun $Co_{36}Fe_{36}Si_{4.8}B1_{9.2}Nb_4$ amorphous alloy

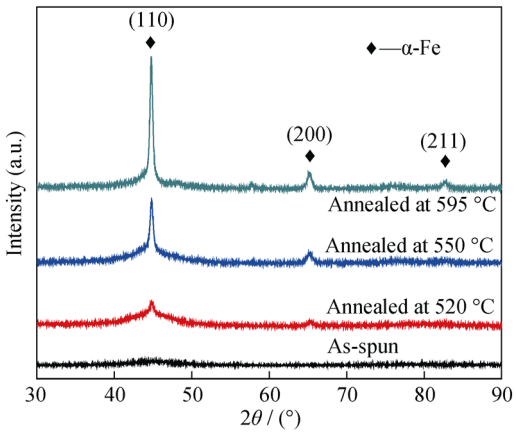

Fig. 3 XRD patterns of $Co_{36}Fe_{36}Si_{4.8}B1_{9.2}Nb_4$ amorphous alloys before and after field annealing at different temperatures with a magnetic field of 9550.0 $A{\cdot}m^{-1}$ for 30 min

indicating that the as-spun alloy is amorphous phase. After the samples were annealed at 520 °C under a transverse magnetic field, the peak at 45° becomes sharp, and a new peak emerges at 65.2° that can be indexed as (200) plane of α-Fe phase, demonstrating that α-Fe phase begins to precipitate, as identified by the standard XRD software (MDI Jade 6.0). When annealing was performed at 550 and 595 °C, another new peak appears at approximately 84 °C, which can be attributed to the (211) plane of α-Fe phase. In addition, the peak becomes sharper with the annealing temperature increasing. The peak widths at half maximums are 1.794°, 0.706° and 0.392° for the alloys annealed at 520, 550 and 595 °C, by which their grain sizes of 4.0, 10.5 and 31.5 nm can be calculated by using the Scherrer equation [19], respectively. Their size changes indicate that the grain sizes of the crystalline phase significantly increase.

Figure 4 shows VSM curves of amorphous alloys annealed at different temperatures in a transverse magnetic field, showing the shape variations of samples with the

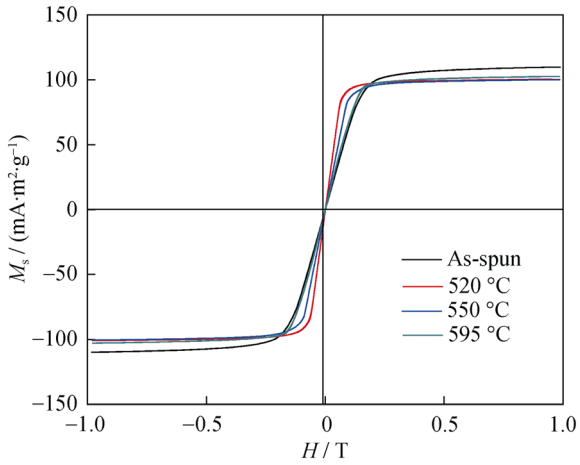

Fig. 4 Hysteresis loops of as-spun $Co_{36}Fe_{36}Si_{4.8}B1_{9.2}Nb_4$ amorphous alloy ribbon and annealed ribbons at 520, 550 and 595 °C in a transverse magnetic field

annealing temperatures increasing. The hysteresis loops of these ribbons can provide typical magnetic parameters, such as the coercivity (H_c), the saturation magnetization (M_s), the residual magnetization (M_r) and the mass susceptivity (χ_m), which are summarized in Table 1. It can be seen from Table 1 that the magnetic properties of the alloy are obviously influenced by the annealing process. The saturation magnetization of the alloy shows a trend of decrease after the first increase with the increase of annealed temperature. The transverse magnetic field has some effect on the magnetic anisotropy, leading to the change of M_s. H_c slowly decreases with the increase of annealed temperature; it can be attributed to the formation of tiny nanocrystallites and microstructure relaxation [20–22]. After annealed at 595 °C, the best magnetic properties of the amorphous alloy are obtained, compared to those of the quenched alloy, M_s increases from 102.9 to 110.00 $mA{\cdot}m^2{\cdot}g^{-1}$, M_r decreases from 0.072 to 0.044 $mA{\cdot}m^2{\cdot}g^{-1}$ and H_c decreases from 78.0 to 57.2 $A{\cdot}m^{-1}$. However, the mass susceptivity (χ_m) reaches its best value of 0.014 $m^3{\cdot}kg^{-1}$ for the sample annealed at 520 °C, which is suitable as the magnetic sensing part.

Hysteresis loops from Fig. 4 suggest that the alloy has excellent soft magnetic property annealed at 595 °C. Therefore, 595 °C was selected as annealing temperature to study the magnetic property of the alloy under three kinds of states such as quenched state, annealed without magnetic field and transverse magnetic field annealing. As shown in Fig. 5, magnetic field annealing has significant effect on the magnetic properties of amorphous alloys. Table 2 gives typical magnetic properties of the sample. After the alloy was annealed in the zero field, its M_s, M_r and H_c all have different degrees of decrease, from 102.9 to 101.4 $mA{\cdot}m^2{\cdot}g^{-1}$ for M_s, from 0.07 to 0.05 $mA{\cdot}m^2{\cdot}g^{-1}$ for

Table 1 Magnetic parameters of as-spun and annealed ribbons at different temperatures

Annealing temperature/°C	M_s/(mA·m^2·g^{-1})	M_r/(mA·m^2·g^{-1})	M_r/M_s	H_c/(A·m^{-1})	χ_m/(m^3·kg^{-1})
As quenched	102.9	0.07	0.0007	78.0	1.32×10^{-2}
520	100.9	0.11	0.0010	65.3	1.42×10^{-2}
550	100.4	0.07	0.0007	63.9	1.37×10^{-2}
595	110.0	0.04	0.0004	57.2	1.32×10^{-2}

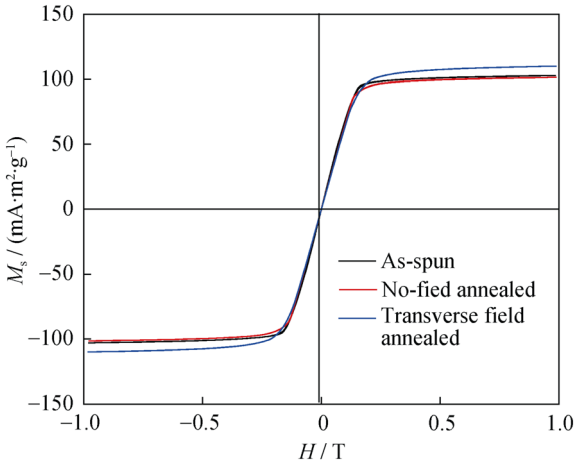

Fig. 5 VSM curves of $Co_{36}Fe_{36}Si_{4.8}B1_{9.2}Nb_4$ amorphous alloys

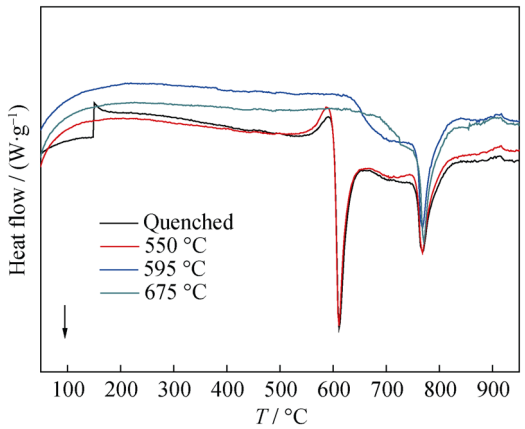

Fig. 6 DSC curves of $Co_{36}Fe_{36}Si_{4.8}B1_{9.2}Nb_4$ amorphous alloys before and after quenching at different temperatures

M_r and from 78.0 to 63.7 A·m^{-1} for H_c. The saturation magnetization of the alloy changes little. Both M_s and M_r have a relatively large decrease since annealing treatment makes the internal stress of the amorphous ribbon fully released, which effectively eliminates the stress-induced magnetic [13, 23]. Moreover, the change of crystal structure or precipitation of crystalline α-Fe phases is another important cause for its magnetic change.

The H_c for the alloy annealed in transverse magnetic field further decreases from 63.7 to 57.3 A·m^{-1} compared with the alloy annealed without field. However, its M_s slightly increases from 101.4 to 110.0 mA·m^2·g^{-1}. The M_s for the alloy annealed in transverse magnetic field is larger than that of as-spun ribbon. In addition, remanence square ratio M_r/M_s for the alloy decreases all the way. When the alloy was annealed under a transverse magnetic field, a minimum H_c, a minimum M_r and a maximum M_s are obtained. H_c decreases to 20.7 A·m^{-1}, M_r decreases to 0.03 mA·m^2·g^{-1} and M_s increases to 7.12 mA·m^2·g^{-1}, respectively, compared with the as-spun ribbon. Evidently, the results show that transverse magnetic field annealing treatment can greatly improve the soft magnetic properties of the alloy, leading to larger M_s and less H_c.

The microstructures modified by the field annealing affect the thermal stability of the alloys. Figure 6 shows DSC curves of these samples after annealing measured by a differential scanning calorimeter (Netzsch 404 °C) at a scanning rate of 20 K·min^{-1}. After annealing at 550 °C, the primary crystallization temperature of the sample slightly decreases from 595 to 588 °C. This change can be attributed to the precipitation of some crystallization phases and the release of inner stress during the annealing [13]. When the annealing temperature increases up to 595 °C, the primary crystallization peak disappears completely, demonstrating the complete precipitation of the first crystalline phase from the alloy. In addition, the secondary

Table 2 Magnetic properties of as-spun ribbons, annealed and magnetic field annealed ribbons at temperature of 595 °C

Samples	M_s/(mA·m^2·g^{-1})	M_r/(mA·m^2·g^{-1})	M_r/M_s	H_c/(A·m^{-1})
As-spun	102.9	0.07	0.0007	78.0
No field annealing	101.4	0.05	0.0005	63.7
Transverse field annealing	110.0	0.04	0.0004	57.2

crystallization temperature (T_{x2}) of the samples annealed at different temperatures is almost coincidental at 749 °C.

Figure 7 shows MF-TGA curves of as-spun alloy and alloys annealed at different temperatures under a transverse magnetic field. These curves can be clearly divided into four stages (AB, BC, CD, DE). The MF-TGA curve of the as-spun alloy shows the magnetic property change of the sample during the heating process, indicating that the sample undergoes several stages. First, based on the AB segment of the curves, the sample preserves a ferromagnetic phase when the temperature increases. At the BC segment, the samples start to change from ferromagnetism to paramagnetism. The starting Point B can be corresponded to the Currie temperature (i.e., T_C = 382 °C for the as-spun sample). From Point D, the crystallization process occurs due to the rapid nucleation and growth, which can improve the ferromagnetic properties of the alloy. The temperature at Point D can be corresponded to the temperature of the second crystalline process in the alloy DSC curve (Fig. 1). During crystallization, the formation of nanocrystals is mainly affected by the initial crystallization temperature (T_{x1}, 595 °C). When the annealing temperature is too high, the thermal and ferromagnetic properties of the alloy can be deteriorated because of the much extensive crystalline phase [24].

Table 3 summarizes the Curie temperature of the alloy ribbons at different temperatures under a transverse magnetic field. The T_C increases first and then decreases with the increase of the annealing temperature, reaching a summit T_C of 440 °C after annealed at 595 °C, which is about 58 °C higher than that of the as-spun alloy. The change of T_C can be correlated with the crystallization of the amorphous alloy [25, 26]. The magnetic properties change little when the annealing temperature is above 755 °C (DE stage) mainly because the compositions, the precipitated crystalline phases and the stress release in the alloys are almost the same after they were annealed at a temperature above T_{x2} (755 °C). The remaining amorphous phase is gradually changed into the crystalline phase at a temperature higher than 755 °C, which can endow the alloy slight ferromagnetic property. After the temperature above 918 °C, the crystalline process is completely done and there are no ferromagnetic domains that could be produced during annealing.

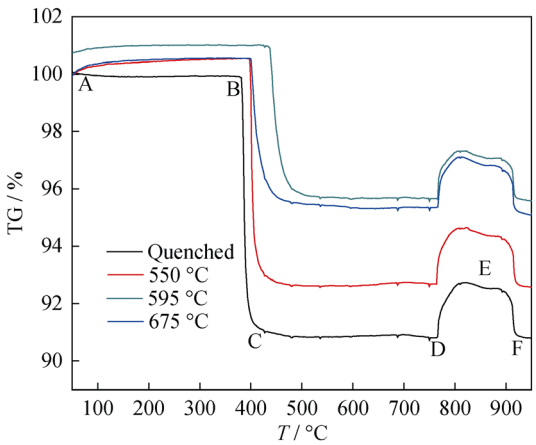

Fig. 7 MF-TGA curves of $Co_{36}Fe_{36}Si_{4.8}B1_{9.2}Nb_4$ amorphous alloy before and after quenching at different temperatures

Table 3 Curie temperature of amorphous alloys annealed at different temperatures

Annealing temperature/°C	Curie temperature/°C
As quenched	382
550	400
595	440
675	405

When the annealing temperature of the alloy increases, the increased T_C may be attributed to the precipitation of the nanoscale ferromagnetic α-Fe(Si) phase (31 nm by XRD measurement) and the enrichment of B atoms in the amorphous phase, which relatively reduces the Fe to B atomic ratio in the remaining amorphous matrix. According to Hasegawa's study on $Fe_{(100-x)}B_x$, the reduction of Fe to B atomic ratio could increase the T_C of the amorphous alloy [27, 28]. The magnetic ordered atoms in α-Fe(Si) and Fe atom undergo electronic exchange coupling effect in the adjacent crystal grains. Thus, magnetic ordering induces the atom diffusion along the interface among the amorphous substrates and the precipitated nanoscale crystalline grains. Consequently, the boundary interfaces among amorphous phases and crystalline grains can undergo spontaneous magnetization at temperatures higher than T_C. In other words, in the annealing process, the thermal activation energy of the interface between the amorphous substrate and the crystalline grains can be enhanced by the exchange coupling effect among nanoscale grains, which can increase the T_C of the sample [29].

When the annealing temperature continues to increase, the size of the α-Fe(Si)-phased crystalline grains increases. The large magnetic–soft α-Fe(Si)-phased grains can deteriorate the ferromagnetic properties of the alloy [30], thus decreasing the T_C of the alloy. In addition, the T_C of the amorphous alloy can be maximized at an optimal annealing temperature. Here, it is 595 °C for $Co_{36}Fe_{36}Si_{4.8}B1_{9.2}Nb_4$, which is related to the precipitation degree and grain size in the annealed alloy.

4 Conclusion

The annealing temperature and magnetic field are two important parameters that affect the magnetic properties of amorphous soft magnetic alloys; the results show that annealing can remove the internal stress of the alloy to a certain extent, thereby reducing the coercive force of the alloy. Under a transverse magnetic field, the coercivity decreases with the increase in the annealing temperature. The saturation magnetization of the field-annealed alloys is improved, and both the residual magnetic induction intensity and the coercivity decrease compared with those of annealed samples without field. After annealing for 30 min at 595 °C in a transverse magnetic field, $Co_{36}Fe_{36}Si_{4.8}B1_{9.2}Nb_4$ amorphous alloy shows excellent soft magnetic properties with an increased saturation magnetization of 110.0 $mA{\cdot}m^2{\cdot}g^{-1}$, a decreased residual magnetic induction intensity of 4×10^{-6} T and a decreased coercivity of 57.3 $A{\cdot}m^{-1}$.

The results show that magnetic field annealing can significantly affect the precipitation of crystalline phases in $Co_{36}Fe_{36}Si_{4.8}B1_{9.2}Nb_4$ amorphous alloy. The DSC curves indicate that the first crystalline phase is precipitated completely after the sample was annealed at 595 °C or higher. After the as-spun alloy was field-annealed at 595 °C for 30 min, the T_C can reach the maximum value of 440 °C, about 58 °C higher than that of the as-spun ribbon (T_C = 382 °C) possibly due to the enhanced saturated magnetism and/or magneto-anisotropy by field annealing.

Acknowledgements This study was financially supported by National S&T Major Project of China (No. 2018ZX10301201), the National Natural Science Foundation of China (No. 51371018) and the Fundamental Research Funds for the Central Universities (No. FRF-BR-14-001B).

References

[1] Yoshizawa Y, Yamauchi K. Effects of magnetic field annealing on magnetic properties in ultrafine crystalline Fe–Cu–Nb–Si–B alloys. IEEE Trans Magn. 1989;25(5):3324.
[2] Kulik T, Ferenc J, Kowalczyk M. Temperature of nanocrystallisation of magnetically soft alloys for high-temperature applications. J Mater Process Technol. 2005;162:215.
[3] Herzer G. Chapter 3, Nanocrystalline Soft Magnetic Alloys. Handbook of Magnetic Materials. Hanau: Elsevier; 1997. 415.
[4] Herzer G. Nanocrystalline soft magnetic materials. J Magn Magn Mater. 1992;112(1):258.
[5] Herzer G. Grain structure and magnetism of nanocrystalline ferromagnets. IEEE Trans Magn. 1989;25(5):3327.
[6] Herzer G. Grain size dependence of coercivity and permeability in nanocrystalline ferromagnets. IEEE Trans Magn. 1990;26(5):1397.
[7] McHenry M, Johnson F, Okumura H, Ohkubo T, Ramanan V, Laughlin D. The kinetics of nanocrystallization and microstructural observations in FINEMET, NANOPERM and HITPERM nanocomposite magnetic materials. Scr Mater. 2003;48(7):881.
[8] Herzer G, Warlimont H. Nanocrystalline soft magnetic materials by partial crystallization of amorphous alloys. Nanostruct Mater. 1992;1(3):263.
[9] Schaefer M, Dietzmann G. Magnetic properties of as-cast and nanocrystallized $Fe_{74.5}Cu_{0.75}Nb_{2.25}Si_{13.5}B_9$ amorphous ribbons. J Magn Magn Mater. 1994;133(1):303.
[10] Willard M, Gingras M, Lee M, Harris V, Laughlin D, McHenry M. Magnetic properties of hitperm (Fe, $Co)_{88}Zr_7B_4Cu_1$ nanocrystalline magnets. In: Proceedings of the MRS Proceedings. San Francisco; 1999. 469.
[11] Willard M, Laughlin D, McHenry M, Thoma D, Sickafus K, Cross JO, Harris V. Structure and magnetic properties of $(Fe_{0.5}Co_{0.5})_{88}Zr_7B_4Cu_1$ nanocrystalline alloys. J Appl Phys. 1998;84(12):6773.
[12] Jiang CB, An SZ. Recent progress in high temperature permanent magnetic materials. Rare Met. 2013;32(5):431.
[13] Tang Z, Song Y, Sun Q, Zhang T, Jiang Y. Magnetic field driving gradient effects on the microstructure in amorphous–nanocrystalline cobalt alloy ribbons. Nanoscale. 2012;4(2):386.
[14] Chiriac H, Marinescu M. Magnetic properties of $Nd_8Fe_{77}Co_5B_6CuNb_3$ melt-spun ribbons. J Appl Phys. 1998;83(11):6628.
[15] Miguel C, Zhukov A, Del Val J, Ramirez de Arellano A, González J. Effect of stress and/or field annealing on the magnetic behavior of the $(Co_{77}Si_{13.5}B_{9.5})_{90}Fe_7Nb_3$ amorphous alloy. J Appl Phys. 2005;97(3):34911.
[16] Zhang S, Sun J, Xing D. Improvement of giant magneto impedance of Co-rich melt extraction wires by stress-current annealing. Rare Met. 2011;30(4):327.
[17] Phan MH, Peng H, Yu SC, Vázquez M. Optimized giant magnetoimpedance effect in amorphous and nanocrystalline materials. J Appl Phys. 2006;99(8):08C505.
[18] Peng H, Qin F, Phan M, Tang J, Panina L, Ipatov M, Zhukova V, Zhukov A, Gonzalez J. Co-based magnetic microwire and field-tunable multifunctional macro-composites. J Non-Cryst Solids. 2009;355(24):1380.
[19] Alexander LE. X-ray Diffraction Procedures for Polycrystalline and Amorphous Materials. 2nd ed. Weinheim: Wiley; 1974. 992.
[20] Škorvánek I, Marcin J, Turčanová J, Wójcik M, Nesteruk K, Janičkovič D, Švec P. Field induced anisotropy and stability of soft magnetic properties towards high temperature in Co-rich nanocrystalline FeCoNbB alloys. J Magn Magn Mater. 2007;310(2):2494.
[21] Marín P, López M, Vlad A, Hernando A, Ruiz-González M, González-Calbet J. Magnetic field driving custom assembly in (FeCo) nanocrystals. Appl Phys Lett. 2006;89(3):033508.
[22] Blázquez J, Roth S, Mickel C, Conde A. Partial substitution of Co and Ge for Fe and B in Fe–Zr–B–Cu alloys: microstructure and soft magnetic applicability at high temperature. Acta Mater. 2005;53(4):1241.
[23] Song Y, Li Z, Sun Q, Tang Z, Zhang T, Jiang Y. Magnetic and electric property evolution of amorphous cobalt–rich alloys driven by field annealing. J Phys D Appl Phys. 2012;45(22):225001.
[24] Knipling KE, Daniil M, Willard MA. Fe-based nanocrystalline soft magnetic alloys for high-temperature applications. Appl Phys Lett. 2009;95(22):222516.
[25] Miguel C, Kaloshkin S, Gonzalez J, Zhukov A. Curie temperature behaviour on annealing of Finemet type amorphous alloys. J Non-Cryst Solids. 2003;329(1–3):63.

[26] Onodera R, Kimura S, Watanabe K, Lee S, Yokoyama Y, Makino A, Koyama K. Magnetic field effects on crystallization of iron-based amorphous alloys. Mater Trans. 2013;54(2):188.
[27] Zhukov A, Blanco J, Gonzalez J, Prieto MG, Pina E, Vazquez M. Induced magnetic anisotropy in Co–Mn–Si–B amorphous microwires. J Appl Phys. 2000;87(3):1402.
[28] Hasegawa R, Ray R. Iron-boron metallic glasses. J Appl Phys. 1978;49(7):4174.
[29] Liebermann H, Graham C, Flanders P. Changes in Curie temperature, physical dimensions, and magnetic anisotropy during annealing of amorphous magnetic alloys. IEEE Trans Magn. 1977;13(5):1541.
[30] Jia P, Wang EG, Han K. The effects of a high magnetic field on the annealing of $[(Fe_{0.5}Co_{0.5})_{0.75}B_{0.2}Si_{0.05}]_{96}Nb_4$ bulk metallic glass. Materials. 2016;9(11):899.